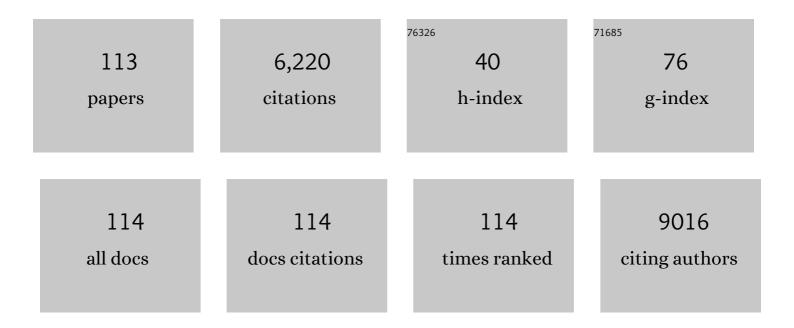
Sun Hee Choi

List of Publications by Year in descending order

Source: https://exaly.com/author-pdf/523337/publications.pdf Version: 2024-02-01



#	Article	IF	CITATIONS
1	Electrochemically Induced Structural Transformation in a γ-MnO ₂ Cathode of a High Capacity Zinc-Ion Battery System. Chemistry of Materials, 2015, 27, 3609-3620.	6.7	788
2	Highly Active and Stable Hydrogen Evolution Electrocatalysts Based on Molybdenum Compounds on Carbon Nanotube–Graphene Hybrid Support. ACS Nano, 2014, 8, 5164-5173.	14.6	531
3	Dry reforming of methane by stable Ni–Mo nanocatalysts on single-crystalline MgO. Science, 2020, 367, 777-781.	12.6	372
4	Influence of Sn content on PtSn/C catalysts for electrooxidation of C1–C3 alcohols: Synthesis, characterization, and electrocatalytic activity. Applied Catalysis B: Environmental, 2008, 82, 89-102.	20.2	261
5	Carbon dioxide Fischer-Tropsch synthesis: A new path to carbon-neutral fuels. Applied Catalysis B: Environmental, 2017, 202, 605-610.	20.2	230
6	Location and State of Pt in Platinized CdS/TiO ₂ Photocatalysts for Hydrogen Production from Water under Visible Light. Journal of Physical Chemistry C, 2008, 112, 17200-17205.	3.1	188
7	Defective ZnFe ₂ O ₄ nanorods with oxygen vacancy for photoelectrochemical water splitting. Nanoscale, 2015, 7, 19144-19151.	5.6	183
8	Topotactic synthesis of mesoporous ZnS and ZnO nanoplates and their photocatalytic activity. Journal of Catalysis, 2008, 254, 144-155.	6.2	144
9	A highly efficient transition metal nitride-based electrocatalyst for oxygen reduction reaction: TiN on a CNT–graphene hybrid support. Journal of Materials Chemistry A, 2013, 1, 8007.	10.3	126
10	Mn-Promoted Ni/Al2O3 Catalysts for Stable Carbon Dioxide Reforming of Methane. Journal of Catalysis, 2002, 209, 6-15.	6.2	124
11	Oxygen-Intercalated CuFeO ₂ Photocathode Fabricated by Hybrid Microwave Annealing for Efficient Solar Hydrogen Production. Chemistry of Materials, 2016, 28, 6054-6061.	6.7	113
12	New Insight into Copper Sulfide Electrocatalysts for Quantum Dot-Sensitized Solar Cells: Composition-Dependent Electrocatalytic Activity and Stability. ACS Applied Materials & Interfaces, 2014, 6, 22078-22087.	8.0	109
13	Activation of Hematite Photoanodes for Solar Water Splitting: Effect of FTO Deformation. Journal of Physical Chemistry C, 2015, 119, 3810-3817.	3.1	108
14	Onset potential behavior in α-Fe ₂ O ₃ photoanodes: the influence of surface and diffusion Sn doping on the surface states. Physical Chemistry Chemical Physics, 2016, 18, 2495-2509.	2.8	96
15	Awakening Solar Water‧plitting Activity of ZnFe ₂ O ₄ Nanorods by Hybrid Microwave Annealing. Advanced Energy Materials, 2015, 5, 1401933.	19.5	95
16	Tree branch-shaped cupric oxide for highly effective photoelectrochemical water reduction. Nanoscale, 2015, 7, 7624-7631.	5.6	90
17	Bifunctional TiO ₂ underlayer for α-Fe ₂ O ₃ nanorod based photoelectrochemical cells: enhanced interface and Ti ⁴⁺ doping. Journal of Materials Chemistry A, 2015, 3, 5007-5013.	10.3	90
18	Sodiumâ€Containing Spinel Zinc Ferrite as a Catalyst Precursor for the Selective Synthesis of Liquid Hydrocarbon Fuels. ChemSusChem, 2017, 10, 4764-4770.	6.8	89

#	Article	IF	CITATIONS
19	X-ray Absorption Fine Structure Characterization of the Local Structure of Fe in Feâ^'ZSM-5. Journal of Physical Chemistry B, 2003, 107, 11843-11851.	2.6	87
20	Mixed Transition Metal Oxide with Vacancy-Induced Lattice Distortion for Enhanced Catalytic Activity of Oxygen Evolution Reaction. ACS Catalysis, 2019, 9, 7099-7108.	11.2	85
21	Fabrication of graphene-based electrode in less than a minute through hybrid microwave annealing. Scientific Reports, 2014, 4, 5492.	3.3	76
22	Sn/Be Sequentially co-doped Hematite Photoanodes for Enhanced Photoelectrochemical Water Oxidation: Effect of Be2+ as co-dopant. Scientific Reports, 2016, 6, 23183.	3.3	75
23	Quantitative Analysis of Tiâ^'Oâ^'Si and Tiâ^'Oâ^'Ti Bonds in Tiâ^'Si Binary Oxides by the Linear Combination of XANES. Journal of Physical Chemistry B, 2000, 104, 8670-8678.	2.6	73
24	Enhancing the catalytic activity of Pt nanoparticles using poly sodium styrene sulfonate stabilized graphene supports for methanol oxidation. Journal of Materials Chemistry A, 2013, 1, 3489.	10.3	73
25	Enhanced Photocatalytic Hydrogen Production from Waterâ^'Methanol Solution by Nickel Intercalated into Titanate Nanotube. Journal of Physical Chemistry C, 2009, 113, 8990-8996.	3.1	72
26	Hydrodechlorination of Carbon Tetrachloride over Pt/MgO. Journal of Catalysis, 1996, 161, 790-797.	6.2	69
27	Subnanometer Cobalt-Hydroxide-Anchored N-Doped Carbon Nanotube Forest for Bifunctional Oxygen Catalyst. ACS Applied Materials & Interfaces, 2016, 8, 1571-1577.	8.0	67
28	Palladium–nickel alloys loaded on tungsten carbide as platinum-free anode electrocatalysts for polymer electrolyte membrane fuel cells. Chemical Communications, 2011, 47, 5792.	4.1	62
29	Phase and photoelectrochemical behavior of solution-processed Fe2O3 nanocrystals for oxidation of water under solar light. Applied Physics Letters, 2008, 93, .	3.3	56
30	Active States of Pd and Cu in Carbon-Supported Wacker-Type Catalysts for Low-Temperature CO Oxidation. Journal of Physical Chemistry B, 2000, 104, 5586-5594.	2.6	52
31	A multitude of modifications strategy of ZnFe2O4 nanorod photoanodes for enhanced photoelectrochemical water splitting activity. Journal of Materials Chemistry A, 2018, 6, 12693-12700.	10.3	52
32	Indium induced band gap tailoring in AgGa1â^'xInxS2 chalcopyrite structure for visible light photocatalysis. Journal of Chemical Physics, 2008, 128, 154717.	3.0	51
33	Trade-off between Zr Passivation and Sn Doping on Hematite Nanorod Photoanodes for Efficient Solar Water Oxidation: Effects of a ZrO ₂ Underlayer and FTO Deformation. ACS Applied Materials & Interfaces, 2016, 8, 19428-19437.	8.0	51
34	Effect of tetravalent dopants on hematite nanostructure for enhanced photoelectrochemical water splitting. Applied Surface Science, 2018, 427, 1203-1212.	6.1	51
35	Fabrication of A/R-TiO 2 composite for enhanced photoelectrochemical performance: Solar hydrogen generation and dye degradation. Applied Surface Science, 2017, 426, 833-843.	6.1	49
36	Effects of Pt Precursors on Hydrodechlorination of Carbon Tetrachloride over Pt/Al2O3. Journal of Catalysis, 1997, 166, 284-293.	6.2	48

#	Article	IF	CITATIONS
37	Exploiting the dynamic Sn diffusion from deformation of FTO to boost the photocurrent performance of hematite photoanodes. Solar Energy Materials and Solar Cells, 2015, 141, 71-79.	6.2	48
38	Highly self-diffused Sn doping in α-Fe ₂ O ₃ nanorod photoanodes initiated from β-FeOOH nanorod/FTO by hydrogen treatment for solar water oxidation. Nanoscale, 2018, 10, 22560-22571.	5.6	47
39	Selective Formation of HÃgg Iron Carbide with g ₃ N ₄ as a Sacrificial Support for Highly Active Fischer–Tropsch Synthesis. ChemCatChem, 2015, 7, 3488-3494.	3.7	46
40	Enhanced Photocatalytic Degradation of Organic Pollutants and Inactivation of <i>Listeria monocytogenes</i> by Visible Light Active Rh–Sb Codoped TiO ₂ Nanorods. ACS Sustainable Chemistry and Engineering, 2018, 6, 4302-4315.	6.7	44
41	Metalâ€Free Artificial Photosynthesis of Carbon Monoxide Using Nâ€Doped ZnTe Nanorod Photocathode Decorated with Nâ€Doped Carbon Electrocatalyst Layer. Advanced Energy Materials, 2018, 8, 1702636.	19.5	42
42	XAFS Study of Tin Modification of Supported Palladium Catalyst for 1,3-Butadiene Hydrogenation in the Presence of 1-Butene. Journal of Catalysis, 2000, 193, 176-185.	6.2	41
43	X-ray Absorption Fine Structure Analysis of the Local Environment of Fe in Fe/Alâ^'MFI. Journal of Physical Chemistry B, 2004, 108, 8970-8975.	2.6	39
44	AgGaS2-type photocatalysts for hydrogen production under visible light: Effects of post-synthetic H2S treatment. Journal of Solid State Chemistry, 2007, 180, 1110-1118.	2.9	36
45	Tunable Photoluminescence across the Visible Spectrum and Photocatalytic Activity of Mixed-Valence Rhenium Oxide Nanoparticles. Journal of the American Chemical Society, 2017, 139, 15088-15093.	13.7	33
46	Supported PdCl2CuCl2 catalysts for carbon monoxide oxidation II. XAFS characterization. Applied Catalysis B: Environmental, 1996, 7, 199-212.	20.2	31
47	The formation of precipitates in the ZnCoO system. Europhysics Letters, 2005, 72, 76-82.	2.0	30
48	Fine-Tuning Pulse Reverse Electrodeposition for Enhanced Photoelectrochemical Water Oxidation Performance of α-Fe ₂ O ₃ Photoanodes. Journal of Physical Chemistry C, 2015, 119, 5281-5292.	3.1	30
49	Enhanced charge transfer with tuning surface state in hematite photoanode integrated by niobium and zirconium co-doping for efficient photoelectrochemical water splitting. Applied Catalysis B: Environmental, 2022, 315, 121538.	20.2	30
50	Role of Graphene Oxide as a Sacrificial Interlayer for Enhanced Photoelectrochemical Water Oxidation of Hematite Nanorods. Journal of Physical Chemistry C, 2015, 119, 19996-20002.	3.1	29
51	Activation of a highly oriented columnar structure of ZnFe2O4 for photoelectrochemical water splitting: Orchestrated effects of two-step quenching and Sn4+ diffusion. Solar Energy Materials and Solar Cells, 2018, 187, 207-218.	6.2	29
52	Synthesis of transparent Zr-doped ZnFe2O4 nanocorals photoanode and its surface modification via Al2O3/Co–Pi for efficient solar water splitting. Applied Surface Science, 2020, 513, 145528.	6.1	29
53	XAFS Characterization of Pt–Mo Bimetallic Catalysts for CO Hydrogenation. Journal of Catalysis, 1997, 167, 364-371.	6.2	28
54	N-Doped ZnS Nanoparticles Prepared through an Inorganicâ^'Organic Hybrid Complex ZnS·(piperazine) _{0.5} . Journal of Physical Chemistry C, 2009, 113, 20445-20451.	3.1	27

#	Article	lF	CITATIONS
55	Porous Zn1-xCdxS nanosheets/ZnO nanorod heterojunction photoanode via self-templated and cadmium ions exchanged conversion of ZnS(HDA)0.5 nanosheets/ZnO nanorod. Chemical Engineering Journal, 2020, 402, 126153.	12.7	27
56	Transparent Zirconium-doped Hematite Nanocoral Photoanode via In-Situ Diluted Hydrothermal Approach for Efficient Solar Water Splitting. Chemical Engineering Journal, 2020, 390, 124504.	12.7	27
57	Magnetron sputtering strategy for Zr-Fe2O3 nanorod photoanode fabricated from ZrOx/β-FeOOH nanorods for photoelectrochemical water splitting. Applied Surface Science, 2021, 549, 149233.	6.1	27
58	Synthesis, electronic property and photocatalytic applications of mesoporous cobalt-doped ZnS and ZnO nanoplates. Applied Catalysis A: General, 2012, 427-428, 106-113.	4.3	26
59	Improved Interfacial Charge Transfer Dynamics and Onset Shift in Nanostructured Hematite Photoanodes via Efficient Ti ⁴⁺ /Sn ⁴⁺ Heterogeneous Self-Doping Through Controlled TiO ₂ Underlayers. ACS Sustainable Chemistry and Engineering, 2019, 7, 6947-6958.	6.7	25
60	Band Gap Tailored Zn(Nb1â^'xVx)2O6 Solid Solutions as Visible Light Photocatalysts. Journal of Physical Chemistry C, 2009, 113, 17824-17830.	3.1	23
61	Lowering the onset potential of Zr-doped hematite nanocoral photoanodes by Al co-doping and surface modification with electrodeposited Co–Pi. Journal of Colloid and Interface Science, 2021, 581, 751-763.	9.4	23
62	Characterization of Pd/C and Cu Catalysts for the Oxidation of Methane to a Methanol Derivative. Journal of Catalysis, 2000, 194, 33-44.	6.2	22
63	Surfactant and TiO 2 underlayer derived porous hematite nanoball array photoanode for enhanced photoelectrochemical water oxidation. Chemical Engineering Journal, 2017, 320, 81-92.	12.7	21
64	A systematic study of post-activation temperature dependence on photoelectrochemical water splitting of one-step synthesized FeOOH CF photoanodes with erratically loaded ZrO ₂ . Sustainable Energy and Fuels, 2021, 5, 3414-3427.	4.9	18
65	XAFS characterization of supported PdCl2â^'CuCl2 catalysts for CO oxidation. Reaction Kinetics and Catalysis Letters, 1996, 57, 227-236.	0.6	17
66	Active size-controlled Ru catalysts for selective CO oxidation in H2. Applied Catalysis B: Environmental, 2012, 127, 129-136.	20.2	17
67	Equilibria, kinetics, and spectroscopic analyses on the uptake of aqueous arsenite by two-line ferrihydrite. Environmental Technology (United Kingdom), 2014, 35, 251-261.	2.2	17
68	Superlattice Formation of Crystal Water in Layered Double Hydroxides for Longâ€Term and Fast Operation of Aqueous Rechargeable Batteries. Advanced Energy Materials, 2018, 8, 1703572.	19.5	17
69	An effective strategy to promote hematite photoanode at low voltage bias via Zr4+/Al3+ codoping and CoOx OER co-catalyst. Electrochimica Acta, 2019, 319, 444-455.	5.2	17
70	A Synergistic Effect of Surfactant and ZrO2 Underlayer on Photocurrent Enhancement and Cathodic Shift of Nanoporous Fe2O3 Photoanode. Scientific Reports, 2016, 6, 32436.	3.3	17
71	Microwave-assisted metal-ion attachment for ex-situ zirconium doping into hematite for enhanced photoelectrochemical water splitting. Renewable Energy, 2022, 189, 694-703.	8.9	17
72	Selective deposition of Pt onto supported metal clusters for fuel cell electrocatalysts. Nanoscale, 2012, 4, 6461.	5.6	16

#	Article	IF	CITATIONS
73	Mechanisms of enhanced sulfur tolerance on samarium (Sm)-doped cerium oxide (CeO ₂) from first principles. Physical Chemistry Chemical Physics, 2014, 16, 10727-10733.	2.8	16
74	Photoelectrochemical, impedance and optical data for self Sn-diffusion doped Fe 2 O 3 photoanodes fabricated at high temperature by one and two-step annealing methods. Data in Brief, 2015, 5, 796-804.	1.0	16
75	High Electrochemical Li Intercalation in Titanate Nanotubes. Journal of Physical Chemistry C, 2009, 113, 14034-14039.	3.1	15
76	Hybrid Microwave Annealing for Fabrication of More Efficient Semiconductor Photoanodes for Solar Water Splitting. ACS Sustainable Chemistry and Engineering, 2019, 7, 944-949.	6.7	15
77	Metal–insulator transition induced by electronic and structural modulations in oxygen-deficient perovskite-type TbBaCo2O5.5. Physica Status Solidi (B): Basic Research, 2006, 243, 1813-1822.	1.5	14
78	Selfâ€ŧemplated fabrication of 2-D dual nanoarchitecture Zn1-xCdxS porous nanosheet and ZnO nanorod for photoelectrochemical hydrogen production. Applied Surface Science, 2021, 539, 148267.	6.1	14
79	Linear combination of XANES for quantitative analysis of Ti–Si binary oxides. Journal of Synchrotron Radiation, 2001, 8, 163-167.	2.4	13
80	Rational design of interface refining through Ti ⁴⁺ /Zr ⁴⁺ diffusion/doping and TiO ₂ /ZrO ₂ surface crowning of ZnFe ₂ O ₄ nanocorals for photoelectrochemical water splitting. Catalysis Science and Technology, 2021, 11, 3141-3152.	4.1	13
81	Synchronized effect of in-situ Ti doping and microwave-assisted SiOx hole transport channel on ZnFe2O4 nanocoral arrays for efficient photoelectrochemical water splitting. Applied Surface Science, 2022, 592, 153212.	6.1	13
82	In-situ synthesis, local structure, photoelectrochemical property of Fe-intercalated titanate nanotube. International Journal of Hydrogen Energy, 2012, 37, 11081-11089.	7.1	12
83	Facile synthesis of Bi2S3 nanosheet/Zr:Fe2O3 nanorod heterojunction: Effect of Ag interlayer on the change transport and photoelectrochemical stability. Journal of Industrial and Engineering Chemistry, 2019, 70, 311-321.	5.8	12
84	Efficient charge transfers in hematite photoanode integrated by fluorine and zirconia co-doping for photoelectrochemical water splitting. Chemical Engineering Journal, 2022, 446, 136957.	12.7	11
85	(111)-Oriented Co0.8Fe2.2O4+δthin film grown by pulsed laser deposition: structural and magnetic properties. Journal of Materials Science, 2013, 48, 6960-6969.	3.7	10
86	Photocatalytic selective oxidation of the terminal methyl group of dodecane with molecular oxygen over atomically dispersed Ti in a mesoporous SiO2 matrix. Green Chemistry, 2013, 15, 3387.	9.0	10
87	Thickness dependent magnetic properties of (111)-oriented Co 0.8 Fe 2.2 O 4 thin film grown by pulsed laser deposition. Thin Solid Films, 2014, 571, 62-68.	1.8	10
88	Enhanced photoelectrochemical performance of internally porous Au-embedded α-Fe ₂ O ₃ photoanodes for water oxidation. Chemical Communications, 2017, 53, 4278-4281.	4.1	10
89	Topotactic and Self-Templated Fabrication of Zn _{1–<i>x</i>} Cd <i>_x</i> Se Porous Nanobelt–ZnO Nanorod for Photoelectrochemical Hydrogen Production. ACS Applied Materials & Interfaces, 2021, 13, 29450-29460.	8.0	10
90	Transesterification of Dimethylcarbonate and Phenol Over Silica Supported TiO2 and Ti-MCM 41 Catalysts: Structure Insensitivity. Catalysis Letters, 2008, 123, 115-122.	2.6	9

#	Article	IF	CITATIONS
91	Sequestration of arsenate from aqueous solution using 2-line ferrihydrite: equilibria, kinetics, and X-ray absorption spectroscopic analysis. Environmental Earth Sciences, 2014, 71, 3307-3318.	2.7	9
92	Insights into the enhanced photoelectrochemical performance of hydrothermally controlled hematite nanostructures for proficient solar water oxidation. Dalton Transactions, 2018, 47, 4076-4086.	3.3	9
93	Effect of low-temperature solvothermal route on controlled growth mechanism of Se rich-ZnSe(en)0.5 templates for ZnO NR-Zn1-xCdxSe photoelectrodes. Applied Catalysis B: Environmental, 2021, 298, 120621.	20.2	9
94	Influence of ZnO Magnetron Sputtering on Controlled Buildout of Zirconium-Doped ZnFe ₂ O ₄ /Fe ₂ O ₃ Heterojunction Photoanodes for Photoelectrochemical Water Splitting. ACS Applied Energy Materials, 2022, 5, 915-929.	5.1	9
95	Structural characterization and effect of dehydration on the Ni-doped titanate nanotubes. Catalysis Today, 2009, 146, 230-233.	4.4	8
96	Detonated growth and functionalization of iron (III) oxyhydroxide nanorod array templates via microwave-assisted synthesis for photoelectrochemical water splitting. Applied Surface Science, 2022, 596, 153609.	6.1	7
97	Microwave-assisted surface attachment of aluminium ions on <i>in situ</i> diluted titanium-doped hematite photoanodes for efficient photoelectrochemical water-splitting. Sustainable Energy and Fuels, 2022, 6, 3056-3067.	4.9	7
98	Luminescence and local structure of Mn-doped ZnS hybrid crystal with two-dimensional platelet morphology. Chemical Physics Letters, 2009, 468, 253-256.	2.6	5
99	XAFS study on Mn-Ni/Al2O3catalyst for carbon dioxide reforming of methane. Journal of Synchrotron Radiation, 2001, 8, 596-598.	2.4	4
100	Correlation between the metal-insulator transition and the electronic density of states near the Fermi level in oxygen-deficient perovskite-type NdBaCo2O5.5. Physica Status Solidi (B): Basic Research, 2005, 242, 1422-1430.	1.5	4
101	Structural Characterization of AgGaS2-type Photocatalysts for Hydrogen Production from Water Under Visible Light. AIP Conference Proceedings, 2007, , .	0.4	4
102	Correlation between displacive-type ferroelectricity and electronic density of states near the Fermi level in SrBi2Ta2O9. Physica Status Solidi (B): Basic Research, 2005, 242, 899-908.	1.5	3
103	Electronic states and local structures of Cu ions in electrodeposited thin films of Cu and Cu2O from X-ray absorption spectra. Physica Status Solidi (B): Basic Research, 2006, 243, 1791-1801.	1.5	3
104	Light-Induced Cleaning of CdS and ZnS Nanoparticles: Superiority to Annealing as a Postsynthetic Treatment of Functional Nanoparticles. Journal of Physical Chemistry C, 2012, 116, 15427-15431.	3.1	3
105	Photocatalytic activity of electron-deficient and porous WO3 nanoparticles derived from thermal oxidation of bulk WC particles. Journal of Photochemistry and Photobiology A: Chemistry, 2016, 330, 37-43.	3.9	3
106	Solid-phase arsenic speciation using XANES: preservation of arsenic species for reliable and accurate environmental risk assessment. International Journal of Environmental Analytical Chemistry, 2020, , 1-18.	3.3	3
107	Effect of Sn-self diffusion via H2 treatment on low temperature activation of hematite photoanodes. Catalysis Science and Technology, 2020, 10, 4245-4255.	4.1	3
108	Photocatalytic synthesis of oxygenated hydrocarbons from diesel fuel for mobile deNOx application. Journal of Catalysis, 2013, 302, 58-66.	6.2	2

#	Article	IF	CITATIONS
109	Reply to Comment on "Quantitative Analysis of Tiâ^'Oâ^'Si and Tiâ^'Oâ^'Ti Bonds in Tiâ^'Si Binary Oxides by the Linear Combination of XANESâ€. Journal of Physical Chemistry B, 2001, 105, 6274-6274.	2.6	1
110	Interactions Between Tetrahydrothiophene (THT) and Silver Species in AgNa-Y. Journal of Nanoscience and Nanotechnology, 2010, 10, 203-210.	0.9	1
111	Response to Comment on "Dry reforming of methane by stable Ni–Mo nanocatalysts on single-crystalline MgO― Science, 2020, 368, .	12.6	1
112	Implementation of Enhanced Quick-scan Technique for Time-Resolved XAFS Experiment at PLS. AIP Conference Proceedings, 2007, , .	0.4	0
113	Observation of slowly decreasing molecular oscillations in ultrathin liquid films using X-ray reflectivity. European Physical Journal: Special Topics, 2009, 167, 163-169.	2.6	0